Materials Characterization 178 (2021) 111290

Contents lists available at ScienceDirect

Materials Characterization

journal homepage: www.elsevier.com/locate/matchar

Characterization of rapidly solidified Al-Mg-Sc alloys with Li addition

T. Gancarz [a,*], A. Dobosz [a], A.-A. Bogno [b], G. Cempura [c], N. Schell [d], R. Chulist [a], H. Henein [b]

[a] Institute of Metallurgy and Materials Science, Polish Academy of Sciences, Reymonta 25 St., 30-059 Krakow, Poland
[b] AMPL, Department of Chemical and Materials Engineering, University of Alberta, Canada
[c] AGH University of Science and Technology, Faculty of Metals Engineering and Industrial Computer Science, 30-059 Krakow, Poland
[d] Institute of Materials Research, Helmholtz-Zentrum Geesthacht, Max-Planck-Strasse 1, D-21502 Geesthacht, Germany

ARTICLE INFO

Keywords:
Aluminium alloys
Rapid solidification
Impulse atomization
Synchrotron diffraction
Intermetallics

ABSTRACT

This paper investigate the thermophysical properties of the liquid as well as the rapid solidification of Al5.0Mg0.2Sc alloys with 3.0 and 6.0 Li wt% by the discharge crucible, and Impulse Atomization techniques respectively. The discharge crucible method, allowed a simultaneous determination of density, surface tension and viscosity as a function of the temperature. While the density and surface tension are found to decrease with Li content, the viscosity increases due to short-range ordering occurring in intermetallic phases. In order to determine their characteristic temperatures, the alloys powder generated by Impulse Atomization were investigated using a Differential Scanning Calorimeter, while microstructural observations and chemical analyses were conducted using scanning and transmission electron microscopy with energy dispersive X-ray spectroscopy. To study the influence of Li on the microstructural phase formation in these alloys, diffraction patterns analyses in transmission electron microscopy, as well X-ray diffraction using synchrotron measurements were carried out. The conducted measurements and microstructure observations revealed the precipitations of Al_3Sc and Al_2MgLi phases in both alloy compositions. In addition, AlLi precipitates were observed in Al5.0Mg0.2Sc6.0Li alloy, which is in agreement with the phase diagram.

1. Introduction

Al alloys (series 2xxx, 5xxx or 7xxx) are attracting renewed interest due to the need for lightweight materials with improved mechanical properties for the aerospace and automotive industries [1,2]. Precipitation hardening in aluminium alloys with the addition of Li, Sc, Zr or Ti is especially attractive, as these alloying elements are light, allow increased strength, and have been applied extensively in the aeronautical and automotive sectors. In order to obtain stable nanoscale precipitates, phase nucleation and diffusion-controlled growth steps are required [3]. Coherency between these strengthening precipitates and the matrix is crucial for mechanical properties, incoherent precipitates result in reduced strength of the material.

Mg is a typical alloying element in solution-strengthened Al alloys. The addition of Mg as a ternary element to Al-Sc alloys leads to improved mechanical properties and nano-structural stability [2,4]. In reference [4], Marquis and co-workers investigated the effects of Mg additions on Al_3Sc precipitation in Al-Sc alloys. The study shows optimisation of the mechanical properties of these multicomponent alloys, and the influence of Mg on creep behaviour of Al(Sc)-based alloys. Their study also indicates that Mg segregation occurs at the perfectly coherent α-Al/Al_3Sc hetero-phase interface, where it is kinetically trapped since Mg is insoluble in Al_3Sc [4]. Consequently, this segregation of Mg leads to a substantial reduction in the anisotropy of the α-Al/Al_3Sc interfacial free energies, which was confirmed by HREM observations [4]. This behaviour is correlated with oversized Mg atoms, 12.08% by radius and 40.82% by volume,in solid solution in the α-Al matrix [5]. In general, Mg addition leads to increased density of Al_3Sc precipitates, with a simultaneous decrease of their coarsening rate [6]. The influence of Mg content from 2 to 6 wt% in Al-Mg-Sc alloys was studied in [7], where it was shown that the mechanical properties increased with Mg content. However, only a slight difference was observed between 4 and 6 wt%. In the case of a Sc addition to aluminium alloys, this element contributes to significantly improving the strength by forming nanoscale coherent $L1_2$-Al_3Sc precipitates [2,4,8] from a supersaturated α-Al solid solution. A high degree of supersaturation leads to an increased driving force, which in turn results in higher density of precipitates [9]. This can be even further increased using rapid solidification techniques. When Li addition to Al alloys is considered, it leads to a drastic reduction of density, accompanied by an increase of elastic modulus. Like with $L1_2$-Al_3Sc in

* Corresponding author.
E-mail address: t.gancarz@imim.pl (T. Gancarz).

https://doi.org/10.1016/j.matchar.2021.111290
Received 3 February 2021; Received in revised form 19 May 2021; Accepted 28 June 2021
Available online 1 July 2021

the Al-Sc system, $AL1_2$-Al_3Li precipitates can form under classical ageing conditions in the Al-Li system. Ternary Al-Mg-Li systems have been studied [1], and it was observed that, during fast quenching to room temperature and low temperature ageing, the Al_3Li phase precipitates were dominant, coherent with the Al matrix. An additional ternary phase (S1-Al_2MgLi) was observed in the system, which mostly nucleated heterogeneously on grain boundaries or dispersions. Mg decreases the solubility of Li in the Al matrix, leading to an enhancement of precipitation in the Al–Mg-Li system, but the interfacial energy of the precipitates is not changed significantly, which is similar to the diffusivity of Li in Al [1,10].

Little work has been done to study the microstructure and phase evolution in Al-Mg-Li-Sc. However, the data indicate that Sc addition increases the stability of the solid solution and the hardenability of alloys containing Li due to the changed Mg/Li proportion in the solid solution [11]. The increase in the cooling rate in quenching increases the capacity for corrosion cracking of Al-Li alloys, which requires restriction of the upper and lower limits of the cooling rate [11]. Al-Mg-Sc-Li alloys are promising Al alloys, as it has been suggested that their mechanical properties exceeds those where Zr was used for microstructure stabilization [12,13].

Al alloys with Mg, Sc and Li additions are attractive for lightweight applications due to the weight of the material, but they have some drawbacks related to Li additions. These include reduction of ductility and fracture toughness after heat-treatment (solution treatment, quenching and ageing) [14]. Rapid solidification could potentially minimize these negative effects by improving the reduced fracture toughness and the low monotonic ductility [14], thus offering unique advantages over conventional solidification processing. In addition to yielding a refine microstructure, it can induce the extension of solid solute solubility above the equilibrium concentration, resulting in a supersaturated solid solution that leads to dispersion strengthening on subsequent upon heat treatment [15]. Using rapid solidification techniques leads to higher toughness, increased hardness, better wear resistance, better fatigue resistance and improved corrosion resistance [16,17]. These enhanced properties result from the non-equilibrium solidification pathway. [16].

In this work, Impulse Atomization (IA), a container-less solidification technique has been used to generate rapidly solidified liquid droplets of Al5.0Mg0.2Sc6.0Li alloy. IA offers a unique opportunity to achieve far-from-equilibrium microstructures through high cooling rates and large undercooling [16,18–21]. IA has the ability to generate several droplets during a single experimental run, with tailored microstructures due to the inherent differences in cooling rate determined by droplet size, atmosphere and superheating [22]. IA has proved to be a reliable to tool for the study of rapid solidification of *Al* alloys. Investigated alloys include Al-Cu [16,23], Al-Cu-Sc [24], Al-Si [25], Al-Fe [19], and Al-Mg-Si [22].

The main objectives of this work are to characterize the thermophysical properties of Al-Mg-Sc-Li melt of two different compositions, and to determine the influence of Li on the microstructures of rapidly solidified droplets obtained by IA. The influence of Mg content from 2 to 6 wt% in Al-Mg-Sc alloys was studied in [7], where it was shown that the mechanical properties increased with Mg content. However, only a slight difference was observed between 4 and 6 wt%. The amount of Sc in the studied compositions was chosen according to investigations in [26], where 0.01 wt% Sc resulted in an improvement of mechanical properties, including yield strength, tensile strength and elongation, and stabilized and shifted the equilibrium of Al-Li phases toward lower temperatures. The presence of Sc leads to a significantly reduced size of the Al_3Li precipitates, but also has a limited effect on the precipitation kinetics, resulting in increased strength in the binary Al-Li system [27,28]. Therefore, the Sc addition influences precipitates depending on composition and thermomechanical processing of Li with the Al and Mg phases. Taking into consideration the reported literature results, an optimal chemical composition, Al-5.0 Mg-0.2Sc with 3.0 and 6.0 wt% of Li is chosen for this study.

2. Experimental

2.1. Material preparation

Al-5.0 Mg-0.2Sc alloys with 3.0 and 6.0 wt% of Li (which corresponds to 10.7 and 19.8 at. %) were prepared by melting high-purity metals (Al, Mg and Sc 99.999%, and Li 99.95%) in a glove-box under a protective atmosphere of high purity argon, with water vapour, nitrogen and oxygen concentration lower than 0.1 ppm to avoid the oxidation of the materials. The atmosphere in the glove-box was additionally purified by Ti shavings, working at 850° C, with a circulation flow rate of 35 m^3/h. The alloys were prepared in an electrical furnace in Al_2O_3 crucibles. *Al* was first melted and homogenized with *Sc* at 1000° C. The temperature was then reduced to 800° C, and Mg and Li were added. The melt was homogenized and then cast onto a steel plate.

2.2. Discharge crucible (DC)

In order to better understand the behaviour of alloys in their liquid state, their thermophysical properties were assessed using the DC method, described in detail elsewhere [29,30]. The alloy was placed in a molybdenum crucible in an electrical furnace. Upon attaining the chosen temperature, the metal was allowed to flow freely from an orifice of fixed radius r_0 at the bottom of the crucible. By measuring the mass flow rate and using numerical solutions based on the relationship between the volumetric flow rate Q, of the liquid exiting the crucible through the orifice, the head of the liquid was calculated using Eq. (1). By solving Eq. (1), the density, viscosity and surface tension could be obtained.

$$h = \frac{1}{2g}\left(\frac{Q}{\left(a_4\left(\frac{2\rho Q}{\pi r_0 \eta}\right)^3 + a_3\left(\frac{2\rho Q}{\pi r_0 \eta}\right)^2 + a_2\left(\frac{2\rho Q}{\pi r_0 \eta}\right) + a_1\right)\pi r_0^2}\right) + \frac{\sigma}{\rho g r_0} \quad (1)$$

where: ρ is the density of liquid (kg/m^3); g is the gravitational acceleration (m/s^2); r_0 is the orifice radius at the bottom of the crucible (m); σ is the surface tension of the melt (mN/m), Q is the liquid free flow rate (m^3/s); η and σ are the melt viscosity and the surface tension, respectively; C_d is the discharge coefficient determined for a given crucible, based on the free flow of liquids with known density; *Re* is the Reynolds number and a_1, a_2, a_3 and a_4 are the coefficients of the polynomial describing Cd versus Re. The crucible and equipment were calibrated using pure *Al*. The measurements were conducted in a temperature range of 650 to 825 °C.

2.3. Thermal analyses by differential scanning calorimetry (DSC)

The thermal histories of the atomized Al-Sc-Mg-Li alloy powders were investigated using a Netzsch DSC 404. The samples (10 mg) were heated and cooled at various rates, including 5, 10, 20 and 40 °C /min, in Al_2O_3 crucibles under a protective atmosphere of high-purity Ar (99.9999%) flowing at 40 ml/min.

2.4. Impulse atomisation

The investigated droplets were produced at the University of Alberta in Edmonton, Canada, using Impulse Atomisation (IA), a drop tube solidification technique developed by AMPL (Advanced Materials & Processing Laboratory). A detail description of the process is given in [31]. The alloys with 3 and 6 at. % of Li prepared in the glove-box (at IMMS PAS in Kraków) were melted in Al_2O_3 crucibles by induction heating under an Ar atmosphere. After 30 min stabilization at 900/ 1000 °C, the melt was impulse atomized in an almost oxygen free (10 ppm)

atomization chamber. The generated droplets were sieved into various size range, ranging from >212 μm to 1000 μm [32]. This wide range of droplets sizes, generated in a single run by IA, provides various thermal histories to be investigated.

2.5. Synchrotron X-ray identification

Phase identification was carried out using X-ray diffraction (XRD). In order to obtain information from the bulk samples, diffraction of high-energy synchrotron radiation (87.1 keV, λ = 0.142342 nm) was performed using a PETRA III P07 beamline at DESY (Hamburg, Germany). Transmission geometry and the high penetration depth of synchrotron radiation SR-XRD allowed diffraction to be obtained from a representative volume of the samples. The diffraction data were collected using an area detector, located at a distance of 1070 mm from the sample, with a beam size of 0.5 × 0.5 mm^2. To ensure that an optimal volume of Al-Mg-Sc-Li alloy was covered by the beam, the sample was measured at three different sites across the interface. The most representative area was chosen for phase analysis. Additionally, to bring all grains into diffraction (all planes fulfilling the Bragg condition), the sample was continuously rotated around the ω axis by $-90° < \omega < 90°$. In such a way, all orientations of a 0.5 × 0.5 × 2 mm sample volume were recorded in one single image.

2.6. Microstructure characterization

Microstructural characterizations of the specimens were carried out using scanning (SEM) and transmission electron microscopy (TEM) techniques. The samples for microstructure observation were grinded and polished in an alcohol solution in order to protect their surfaces, and were coated with carbon in order to avoid oxidation. Specimens were investigated using SEM prior to TEM lamella preparation. During SEM investigation a specified area for targeted specimen preparation was selected. Then, TEM lamella was prepared using focused ion beam (FIB). Phase identification was performed using selected area electron diffraction (SAED), using TEM and confirmed with X-ray diffraction (XRD) [33]. Chemical microanalysis was conducted using the energy dispersive X-ray spectroscopy (EDS) technique. Additional characterization of phase distribution was performed by high angle annular dark field (HAADF-STEM). Phase identification was achieved through selected area electron diffraction techniques (SAED), using TEM and confirmed with X-ray diffraction (XRD).

3. Results and discussion

3.1. Thermophysical properties of the investigated Al-Mg-Sc-Li melts

Using the DC method, the density, viscosity and surface tension of Al-Mg-Sc-Li alloys were investigated (see Fig. 1). The obtained temperature dependence of density (Fig. 1a) and surface tension (Fig. 1b) were described by linear equations, and the viscosity (Fig. 1c) by an Arrhenius type equation (Table 1). Density and surface tension data were described by the linear equations ($Y(T) = a + b \cdot T$), and for viscosity the Arrhenius equation ($\eta = A \cdot e^{\frac{E}{RT}}$) was used. Where Y is γ – surface tension or ρ – density, and *a, b* is linear parameters; η – viscosity, A, E – coefficients, R – gas constant, T – temperature. Table 1 includes the parameters of the equations, along with estimated standard deviation of the equation parameters, and values calculated at 700 °C. The lines for density and surface tension and the Arrhenius equation for viscosity were in good agreement with the experimental data, and the parameter $R^2 = 0.988 \div 0.999$.

The density and surface tension of Al-Mg-Sc-Li alloys decreased as Li content increased, while for viscosity an opposite trend was observed. The obtained results are similar to those for the Al-Li system, where the same character of change is observed [34]. The decrease of density and increase of viscosity are correlated with short-range ordering in the liquid occurring from the formation of IMCs, as confirmed by the results described in Section 3.3. The obtained results for pure *Al* show very good agreement with the literature data according to the last review by Assael et al. [35], where the difference between the proposed equation and experimental results was below 1%. The results of density and viscosity were also compared with a similar composition (Al4.6Mg0.66Sc0.42Zr0.49Mn [36]), but it should be noted that those results were obtained by computational simulation using numerical models.

The calculated density for Al4.6Mg0.66Sc0.42Zr0.49Mn [36] using linear thermal expansion was similar to that obtained for Al5.0Mg0.2Sc3.0Li alloy. The calculated values for surface tension of Al4.6Mg0.66Sc0.42Zr0.49Mn alloy [36] are much higher 977 $mN \cdot m^{-1}$, compared to data obtained in this study (723.1 $mN \cdot m^{-1}$ for Al5.0Mg0.2Sc3.0Li and 632.6 $mN \cdot m^{-1}$ for Al5.0Mg0.2Sc6.0Li, at a temperature of 900 °C). The higher values could be explained by the fact that the *Al* surface tension data for calculations were taken from [38]. The alloying elements and increasing Li in alloys caused an increase in viscosity, compared to pure Al, which is inconsistent with the data for Al4.6Mg0.66Sc0.42Zr0.49Mn alloy [36], where the calculated viscosity data are lower. This could be the result of a lower value of viscosities for pure elements. However it is important to note that the trend observed in this study is in agreement with the increase of viscosity observed in Al-Li [34]. The higher values of viscosity are caused by the formation of IMCs from the Al-Li system, correlated with short-range ordering in the liquid which was confirmed by measurements and modelling [34].

3.2. Thermal analyses of the investigated alloys

DSC results are presented in Fig. 2 as heating (a) and cooling (b)

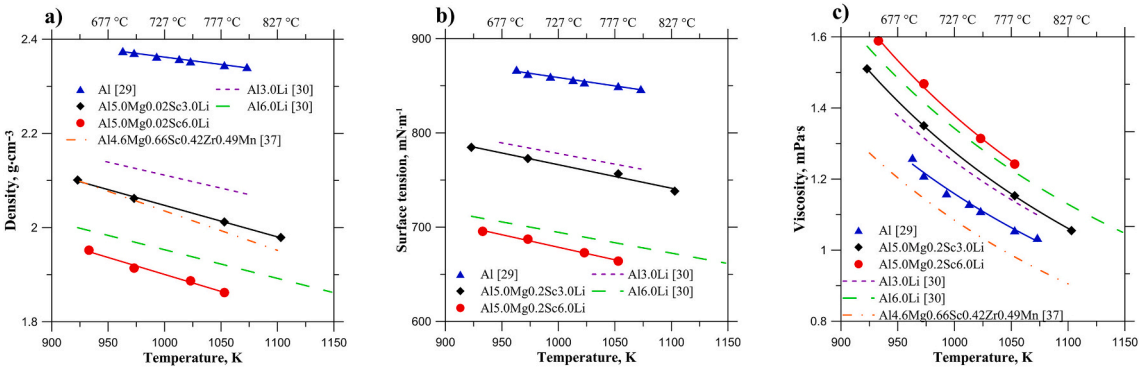

Fig. 1. The temperature dependency of a) density, b) surface tension and c) viscosity of Al-Mg-Sc-Li alloys compared with literature data for Al [37], Al-Li alloys [34], and Al4.6Mg0.66Sc0.42Zr0.49Mn [36].

Table 1
The A, B, E_a coefficients[a,b,c] and their standard deviation of the linear temperature dependence of density and surface tension, and the Arrhenius equation described viscosity for Al-Mg-Sc-Li alloys, and calculated values at 700 °C.

Density						
Alloys	A ($g \cdot cm^{-3}$)	u (A)	B ($g \cdot cm^{-3} T^{-1}$)	u (B)	ρ (700 °C) ($g \cdot cm^{-3}$)	s (ρ)
Al [29]	2.674		−0.0003		2.371	
Al5.0Mg0.2Sc3.0Li	2.72	0.02	−0.00067	0.00002	2.233	0.003
Al5.0Mg0.2Sc6.0Li	2.62	0.06	−0.00072	0.00006	2.100	0.006
Surface tension						
Alloys	A ($mN \cdot m^{-1}$)	u (A)	B ($mN \cdot m^{-1} \cdot T^{-1}$)	u (B)	σ (700 °C) ($mN \cdot m^{-1}$)	s (σ)
Al [29]	1036.10		−0.18		863.40	
Al5.0Mg0.2Sc3.0Li	1015.3	22.4	−0.249	0.022	772.9	0.2
Al5.0Mg0.2Sc6.0Li	944.7	13.9	−0.266	0.014	685.8	1.4
Viscosity						
Alloys	A ($Pa \cdot s$)	u (A)	E_a ($J \cdot mol^{-1}$)	u (E_a)	η (700 °C) ($Pa \cdot s$)	s (η)
Al [29]	0.191		14,982.4		1.277	
Al5.0Mg0.2Sc3.0Li	0.168	0.006	16,834.5	34.6	1.349	−0.001
Al5.0Mg0.2Sc6.0Li	0.181	0.010	16,882.9	45.3	1.458	−0.010

[a] Estimated from linear regression error as implemented in the Grapher Software Package.

[b] Estimated from difference computed between experimental and calculated from linear density fit, $s(m) = \frac{1}{N}\sum_{i=1}^{N}|m^{exp} - m^{fit}|$, where N is the number of experimental points and standard deviation of density s(ρ), surface tension s(σ) and viscosity s(η).

[c] Standard uncertainties u are u(T) = 1 K, u(p) = 0.1 kPa at atmospheric pressure p = 0.1 MPa, w(X) = 0.0001 for *Al*, Mg and w(X) = 0.001 for *Sc*, Li.

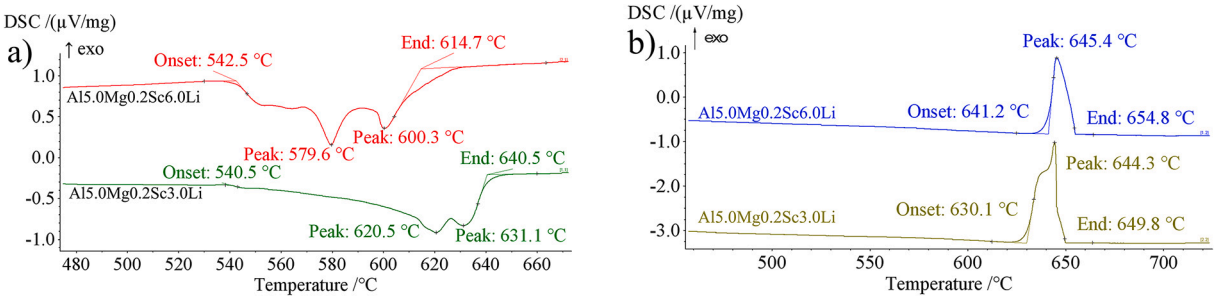

Fig. 2. The DSC curves vs. temperature for Al-Mg-Sc-Li alloys: a) during heating, b) cooling conditions.

curves. The addition of 5 wt% of Mg to Al caused a characteristic reaction from the Al-Li-Mg system. The obtained results are in good agreement with literature data for the Al-Li-Mg system [39–43]. The phase diagrams Al-Li [40,41] and Al-Li-Mg [42], are presented in Fig. 3, with the corresponding chemical composition of investigated alloys.

For both alloys, with 3 and 6 wt% of Li, the first reaction can be noticed on the calorimetry curve at around 540 °C, and corresponds with the beginning of the dissolving of the ternary Al_2LiMg phase. The reaction can be written as: L + AlLi <≥ (*Al*) + Al_2LiMg at 536 °C [43]. The next DSC signals occur at different temperatures and are dependent on the amount of Li in the system, which is correlated with the phase diagrams (Fig. 3). For 3 wt% of Li in the Al-Mg-Sc alloy, the next peaks are observed at ~620 and ~631 °C, which represents (Fig. 3a) the transformation from the (*Al*) + L semisolid phase to the liquid L phase. For Al-Mg-Sc alloys with 6 wt% of Li content, different reactions were observed compared to 3 wt% Li. The two peaks appear, but at lower temperatures. The first peak, at ~580 °C, could correspond with the eutectic reaction from the Li-Mg system L < => (Mg) + (Li) at 588 °C [44–46]. The peak around 600 °C represents the eutectic reaction in the Al-Li system, L < => (A1) + AlLi, which was observed at 600 °C [40], 602 °C [43] or 596 °C [45] in previous works.

During cooling (Fig. 2b), a crystallization peak was observed for both Li additions. The peaks are close to the melting point of *Al*, as shown in Fig. 3. The expansion of the peak for Al-Mg-Sc with 6 wt% Li reflects the higher concentration of Li in the alloy. There is no effect after crystallization, which means that the effect obtained during heating is correlated with the rapid solidification process during droplet production. In the ternary Al-Li-Mg alloys, according to the phase diagram shown in Fig. 3b, the equilibrium structure consists of (*Al*) grains with secondary particles of *Al* and Al_2LiMg phases formed during cooling in the solid

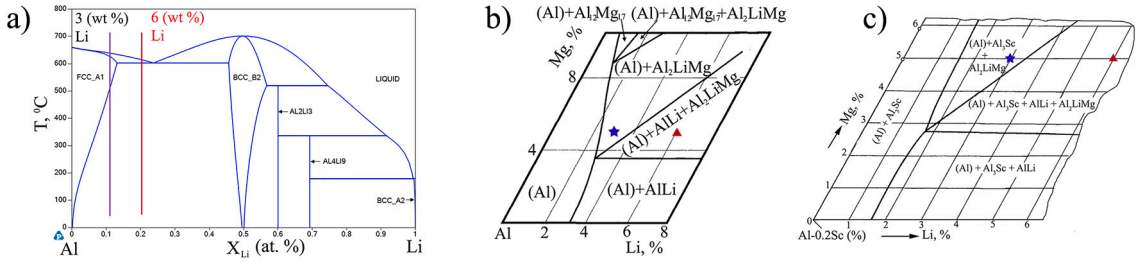

Fig. 3. The phase diagram of a) Al-Li [41,42] and b) isothermal section of Al-Li-Mg at 500 °C [43] and c) isothermal section of Al0.2Sc-Li-Mg at 400 °C [8] with the signed chemical composition of investigated alloys.

state. The magnesium at early stages of decomposition decreases the solid solubility of Li, which in turn increases the density of precipitation of AlLi. Moreover, Mg and Li form the ternary compound Al_2LiMg, which is incoherent and nucleates on grain boundaries or dislocation networks. However, taking into account the chemical composition of alloys with 0.2 *Sc* wt%, the Al_3Sc phase should be present, according to the phase diagram in Fig. 3c. The chemical composition of the studied alloys corresponds with Al5.0Mg0.2Sc3.0Li alloy in the region of (*Al*) + Al_3Sc + Al_2LiMg, and with Al5.0Mg0.2Sc6.0Li alloy in the (*Al*) + Al_3Sc + AlLi + Al_2LiMg region. *Sc* addition causes the stabilization of the structure, considerably slowing down lithium diffusion and coarsening of Al_3Li or AlLi phases. In addition, it stabilizes the Al_2LiMg phase, which could be created at higher Li concentrations. Moreover, the presence in the structure of coherent or semicoherent Al_3Sc (cubic particles) provides places for preferential nucleation of the Al-Li phases.

The Al5.0Mg0.2Sc6.0Li was additionally analyzed at different heating rates. In this case, characteristic reactions were observed at much lower temperatures than the main peak. The first peak corresponds with the eutectic reaction at 418 °C – L < => (Mg) + $Mg_{17}Al_{12}$ + AlLi [43]. The second peak starts at around 485 °C, which matches the invariant reaction U_2 [43] at 483 °C, L + Al_2LiMg < => (*Al*) + $Mg_{17}Al_{12}$. Increasing the heating rate from 5 to 40 °C/min results in a slight shift of the characteristic reaction peak toward lower temperatures. This could be connected with the mentioned precipitates from the Al-Sc-Li-Mg system in the microstructure, which are described in the next section.

3.3. Microstructure and phase analysis

The microstructures of the obtained droplets are presented in Fig. 4 a), b) for Al5.0Mg0.2Sc3.0Li alloy and c), d) for Al5.0Mg0.2Sc6.0Li alloy, respectively. There are major differences in the microstructure of the studied alloys. In the case of the alloy with 6 wt% Li, more precipitates are observed compared to Al5.0Mg0.2Sc3.0Li. The obtained microstructure for Al5.0Mg0.2Sc3.0Li alloy after rapid solidification looks very similar to the microstructure obtained after the solution was treated at 570 °C for 20 h [47]. As shown in [48], the microstructures of cast ingots exhibiting ternary peritectic reactions are often typical of non-equilibrium type reactions in the material. In this case, a second phase forms around the primary phase, as shown in Fig. 2b. In the case of a Scheil-type micro-segregation, the final composition of the solidification can be meaningfully predicted [49] which could go along the monovariant lines as was analyzed in [50] for the Al-Li-Cu system.

The observed characteristics effect of inclusion in relation to grain boundary (GB) in the second phase, created in the structure, as shown in Fig. 5b and d, in the grain boundary occurring the appearing dark-grey phase is fully or partially surrounds by second phase light-grey. During solidify the complete and incomplete wetting of grain boundaries by the melt or second solid phase make occur, as observed in [51], the formation of coherent and semicoherent particles of metastable phases in our case Al2Mg. Other hand, the increasing Li content caused formation AlLi precipitates in Al (Fig. 5d) inside in Al grains, what it can even prevent segregation Li to GBs. A more detailed discussion of the effect of co-segregation, however, requires a separate investigation, and is outside the scope of the present study.

In the microstructure of Al5.0Mg0.2Sc3.0Li, an Al matrix with small precipitates Al_3Sc and Al_2Mg and Mg rich phases on the grain boundary is observed (Fig. 5). The secondary electron micrographs and EDS elemental maps for Al, Mg, and Sc were prepared. On the EDS maps, the dispersion of *Sc* in the entire volume of the sample is apparent. The Al formed grains and Mg occurred at the grain boundary, just as observed in [36].

The conducted chemical analysis in SEM for Al5.0Mg0.2Sc3.0Li alloy, presented in Fig. 5, shows that Mg is present at the grain boundary, while Sc is distributed throughout the volume and is also partially located at grain boundaries. The same *Sc* distribution was observed in [52] for Al5Mg0.2Sc cast alloy, but with increasing *Sc* content to 0.4–0.6, which caused the formation of small square precipitates of Al_3Sc. However, the presence of Al_3Sc precipitates should be more visible after heat treatment, as shown in the literature data [36,53]. Moreover, the addition of 0.2 Mg and 5.0 wt% resulted in the formation of the Al_3Sc phase, which is in agreement with the phase diagram of Al-Mg-Sc [2]. However, the addition of Li introduces changes in the observed phases (Fig. 3c) [54]. In the case of the microstructure of the Al5.0Mg0.2Sc6.0Li alloy (Fig. 4d), a higher density of small precipitates is observed. This, together with increased Li content, caused the formation of the AlLi phase precipitates, in accordance with the phase diagram (Fig. 3c) [54].

The TEM observations of Al5.0Mg0.2Sc6.0Li alloy, presented in Fig. 6, show the presence of small IMC precipitates at grain boundaries of Al grains and Mg regions. A similar microstructure was obtained in [55], where Mg addition caused substantial grain refinement of aluminium, while Sc formed a very fine dispersion of Al_3Sc precipitates, which is very efficient in restricting the grain growth. The precipitates in Fig. 6 are potentially AlLi and Al_2MgLi phases, which were identified by SR-XRDs, presented in Fig. 9.

The conducted HAADF in TEM presented in Fig. 7 shows the maps of concentration of elements present in the sample. The observed Mg regions (Fig. 7c) are dendritic-like with diffused shapes of varying sizes, enriched in *Al*. Taking into account that the characterization of Li is difficult using HAADF-STEM, the presence of AlLi and Al_2MgLi phases was confirmed by electron diffraction patterns using TEM and SR-XRDs. Similar precipitates to AlLi presented in Fig. 6 were observed by Noble and Thompson [56] and Prasad et al. [57]. In the case of the Al_2MgLi phase, as reported in [52–54,59], the precipitates located at the interdendrite spaces between the dendrite branches have a high enrichment of aluminium. The alloys with Li additions show two types of nucleation mechanisms unique for alloys with Li content [57]. The first mechanism is the nucleation on the AlLi phase present at the matrix interface. In this case, Mg concentration occurs at the growth front. This, combined with the excess vacancies released when Li adds to the AlLi precipitate, results in favourable conditions for Al_2MgLi nucleation. The second nucleation mechanism is when the nucleation occurs on matrix dislocations and on sub-grain boundary dislocations [57]. Therefore, as shown in the phase diagram in Fig. 3 and by Fridlyander et al. [59], who studied the addition of Li and Mg, the solubility of Sc in Al is decreased, and this in turns promotes the formation of Al_3Sc. The grain size and shape are also affected by the casting variables, such as cooling rate, superheating of the melt, and stirring.

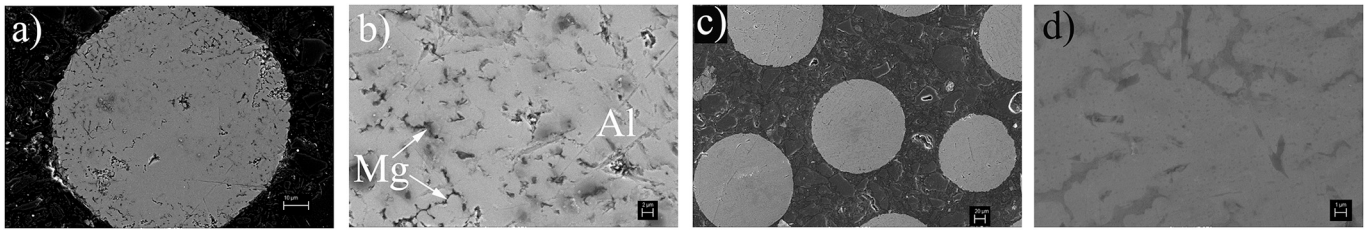

Fig. 4. SEM microstructures of droplets a) and b) Al5.0Mg0.2Sc3.0Li with higher magnification, c) and d) Al5.0Mg0.2Sc6.0Li with higher magnification.

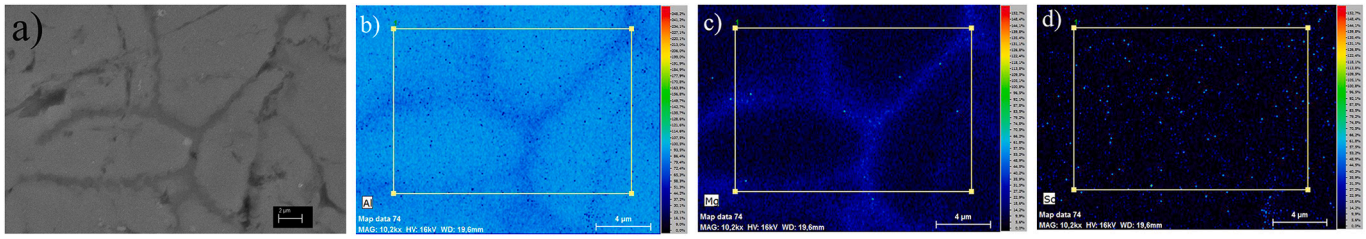

Fig. 5. SEM microstructures (a) and EDS maps of Al5.0Mg0.2Sc3.0Li alloy: b) Al, c) Mg and d) Sc.

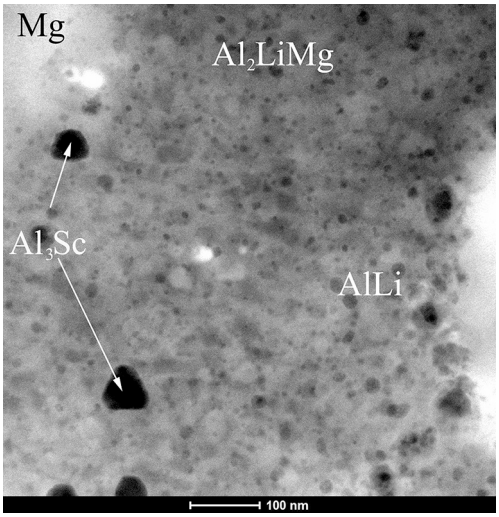

Fig. 6. The microstructure HAADF in TEM of Al5.0Mg0.2Sc6.0Li alloy.

The phases after atomization (Fig. 8) were identified with the use of the phase diagram presented in Fig. 3, and using data presented in the literature [48,52,53,56,59]. The crystallographic structure of the Al_3Sc phase was taken from [61], for AlLi from [62] and for Al_2Mg from [62]. Fig. 8 shows the selected area diffraction (SAED) and electron diffraction patterns of Al5.0Mg0.2Sc3.0Li alloy, identifying the precipitates as Al_3Sc, AlLi and Al_2Mg phases, which matches the prediction based on the phase diagram in Fig. 3c.

The SR-XRD measurements were conducted for Al5.0Mg0.2Sc3.0Li and two sizes of Al5.0Mg0.2Sc6.0Li droplets in order to determine whether the size of the droplets is correlated with changes in the phase composition of the alloy. The droplets were fine (425–500 µm) and coarse (1.18–1.4 mm). The results are presented for Al5.0Mg0.2Sc6.0Li alloys (for two droplet sizes) and for Al5.0Mg0.2Sc3.0Li alloy in Fig. 9. In order to analyze the obtained SRXRD results and attribute the peak to phases, higher magnification was needed, where the highest peak from Al was omitted, as shown in Fig. 9b. The SRXRD shows that, for Al5.0Mg0.2Sc3.0Li alloy, the AlLi phase was not present, and the characteristic peaks from the Al_2MgLi phase seem to be shifted and correspond to the Al_2Mg phase. The cell parameters for Al_2MgLi phase taken from [52,56,59,60,63,64] suggest that a = 20.2 Å, although the equilibrium between Al or Mg and AlLi can affect that parameter and could increase it up to 1.5%.

4. Conclusions

In this study, experimental investigations of Al-Mg-Sc-Li were carried out to show the influence of Li on the thermophysical properties of liquid by the discharge crucible method, and the rapid solidification microstructures of the alloys obtained by rapid solidification.

The following conclusions could be drawn:

1. The density and surface tension decrease as Li content increases, while the opposite is observed for viscosity. The higher value of viscosity compared to Al-Li alloys could be caused by the formation of IMCs not only from the Al-Li system, but also from a ternary phase such as Al_2MgLi.

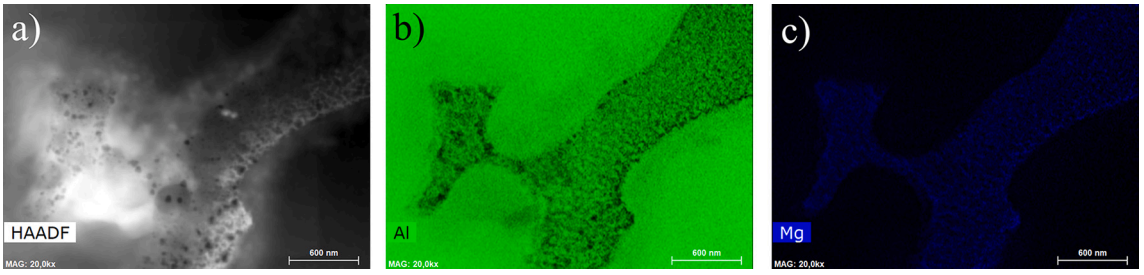

Fig. 7. A) HAADF-STEM image of Al5.0Mg0.2Sc6.0Li alloy and corresponding EDS maps for b) Al, c) Mg concentration.

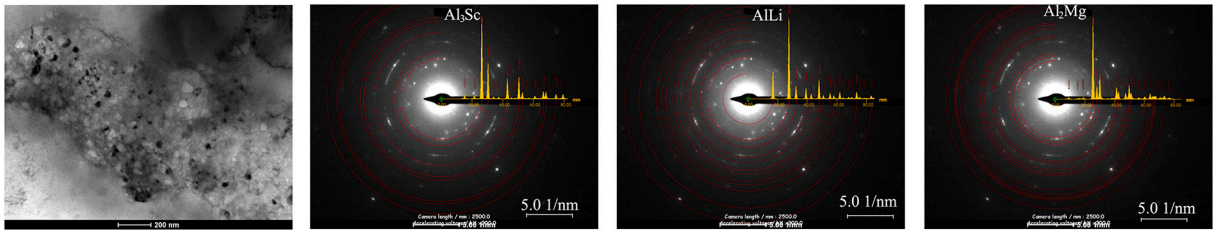

Fig. 8. The microstructure of Al5.0Mg0.2Sc3.0Li alloy as identified by SAED and electron diffraction patterns of the Al_3Sc, AlLi, and Al_2Mg phases.

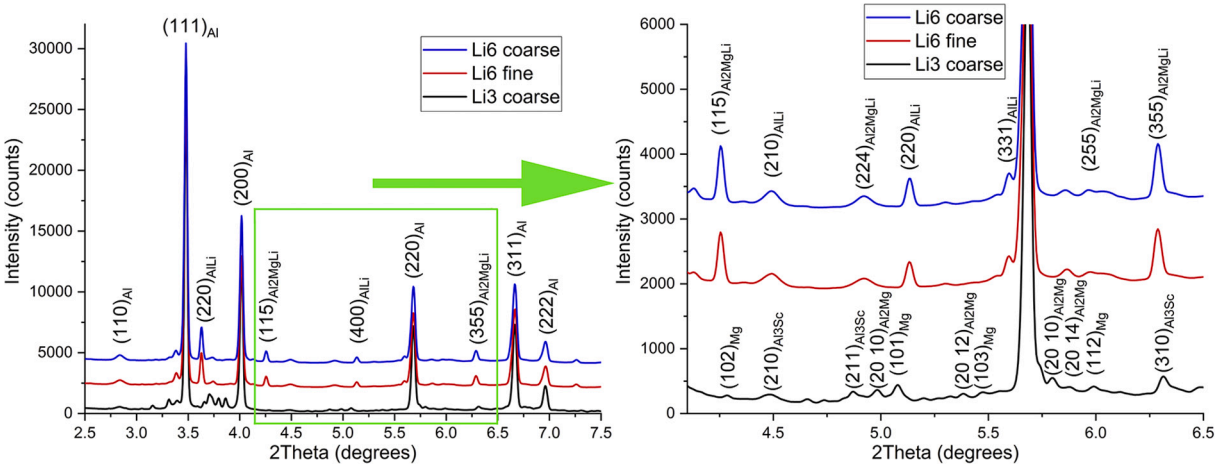

Fig. 9. The SR-XRD result for Al5.0Mg0.2Sc3.0Li and Al5.0Mg0.2Sc6.0Li alloys.

2. The presence of the Al_2MgLi phase was confirmed by SR-XRDs. The obtained results are in line with the phase diagram of Al-Li-Mg system (Fig. 3) and with the literature [43,50,58].
3. The generated Al5.0Mg0.2Sc3.0Li droplets after atomization were characterized by the presence of Al_3Sc and Al_2MgLi phases at grain boundaries of *Al* grains. The microstructure observation for Al5.0Mg0.2Sc6.0Li alloy showed the existence of another AlLi phase as small precipitates inside the *Al* grains.
4. The thermal analysis by DSC showed a similar character of temperature phase transformations. However, there are specific differences between the obtained DSC curves for Al5.0Mg0.2Sc3.0Li and Al5.0Mg0.2Sc6.0Li alloys. The obtained results are in agreement with the phase diagram of the Al-Li-Mg system proposed by [43], presented in Fig. 3
5. The IMCs Al_3Sc, AlLi and Al_2MgLi phases were confirmed by electron diffraction patterns in TEM and SR-XRDs.
6. Rapid solidification of Al-Mg-Sc-Li alloys with 6 wt% of Li was successfully achieved by Impulse Atomization. The generated rapid solidification microstructures and phase composition, showed great potential for powder feedstock to be used in processes such as additive manufacturing. These microstructures can still be improved by choosing the right parameters for higher undercooling to generate more metastability in the solidification path.

Declaration of Competing Interest

The authors declare that they have no known competing financial interests or personal relationships that could have appeared to influence the work reported in this paper.

Acknowledgment

This work is the result of cooperation between the Department of Chemical and Materials Engineering, University of Alberta and the Institute of Metallurgy and Materials Science, Polish Academy of Sciences. “The support of the Natural Sciences and Engineering Research Council is gratefully acknowledged”.

References

[1] A. Deschamps, C. Sigli, T. Mourey, F. De Geuser, W. Lefebvre, B. Davo, Experimental and modelling assessment of precipitation kinetics in an Al-Li-Mg alloy, Acta Mater. (2012), https://doi.org/10.1016/j.actamat.2012.01.010.
[2] J. Røyset, N. Ryum, Scandium in Aluminium Alloys, 2005, https://doi.org/10.1179/174328005X14311.
[3] A. Deschamps, G. Fribourg, Y. Bréchet, J.L. Chemin, C.R. Hutchinson, In situ evaluation of dynamic precipitation during plastic straining of an Al-Zn-Mg-Cu alloy, Acta Mater. 60 (2012) 1905–1916, https://doi.org/10.1016/j.actamat.2012.01.002.
[4] E.A. Marquis, D.N. Seidman, M. Asta, C. Woodward, Composition evolution of nanoscale Al3Sc precipitates in an Al-Mg-Sc alloy: experiments and computations, Acta Mater. (2006), https://doi.org/10.1016/j.actamat.2005.08.035.
[5] H.W. King, Quantitative size-factors for metallic solid solutions, J. Mater. Sci. 1 (1966) 79–90, https://doi.org/10.1007/BF00549722.
[6] P. Xu, F. Jiang, M. Tong, Z. Tang, J. Jiang, N. Yan, Y. Peng, Precipitation characteristics and morphological transitions of Al3Sc precipitates, J. Alloys Compd. 790 (2019) 509–516, https://doi.org/10.1016/j.jallcom.2019.03.256.
[7] R.R. Sawtell, C.L. Jensen, Mechanical properties and microstructures of Al-Mg-Sc alloys, Metall. Trans. A. 21 (1990) 421–430, https://doi.org/10.1007/BF02782422.
[8] L.S. Toropova, D.G. Eskin, M.L. Kharakterova, T.V. Dobatkina, Advanced Aluminum Alloys Containing Scandium-Structure and Properties, Gordon and Breach Science Publishers, Amsterdam, Netherlands, 1998.
[9] J. Taendl, A. Orthacker, H. Amenitsch, G. Kothleitner, C. Poletti, Influence of the degree of scandium supersaturation on the precipitation kinetics of rapidly solidified Al-Mg-Sc-Zr alloys, Acta Mater. (2016), https://doi.org/10.1016/j.actamat.2016.07.001.
[10] A. Abd El-Aty, Y. Xu, X. Guo, S.H. Zhang, Y. Ma, D. Chen, Strengthening mechanisms, deformation behavior, and anisotropic mechanical properties of Al-Li alloys: a review, J. Adv. Res. 10 (2018) 49–67, https://doi.org/10.1016/j.jare.2017.12.004.
[11] G.L. Shneider, A.M. Drits, Hardenability of aluminum-lithium alloys, M Sci. Heat Treat. 37 (1995) 373–377, https://doi.org/10.1007/BF01156813.
[12] A. Lawley, An overview of powder atomization processes and fundamentals, Int. J. Powder Metall. 13 (1977) 169–188.
[13] R.A. Emigh, The Aluminum-Scandium-Lithium-Magnesium System as a Potential Source of Superplastically Formable Alloys, 1990.
[14] E.J. Lavernia, T.S. Srivatsan, F.A. Mohamed, Strength, deformation, fracture behaviour and ductility of aluminium-lithium alloys, J. Mater. Sci. 25 (1990) 1137–1158, https://doi.org/10.1007/BF00585420.
[15] D.W. Heard, J. Boselli, R. Rioja, E.A. Marquis, R. Gauvin, M. Brochu, Interfacial morphology development and solute trapping behavior during rapid solidification of an Al-Li-Cu alloy, Acta Mater. 61 (2013) 1571–1580, https://doi.org/10.1016/j.actamat.2012.11.034.
[16] M. Bedel, G. Reinhart, A.A. Bogno, C.A. Gandin, S. Jacomet, E. Boller, H. Nguyen-Thi, H. Henein, Characterization of dendrite morphologies in rapidly solidified Al-4.5 wt.%Cu droplets, Acta Mater. (2015), https://doi.org/10.1016/j.actamat.2015.02.007.
[17] J.E. Hatch (Ed.), Aluminum: Properties and Physical Metallurgy, ASM International, 1984.
[18] A. Prasad, H. Henein, E. Maire, C.A. Gandin, Understanding the rapid solidification of Al-4.3Cu and Al-17Cu using X-ray tomography, Metall. Mater. Trans. A Phys. Metall. Mater. Sci 37 (2006) 249–257, https://doi.org/10.1007/s11661-006-0170-3.
[19] H. Henein, V. Buchoud, R.R. Schmidt, C. Watt, D. Malakhor, C.A. Gandin, G. Lesoult, V. Uhlenwinkel, Droplet solidification of impulse atomized Al-0.61Fe and Al-1.9Fe, Can. Metall. Q. 49 (2010) 275–292, https://doi.org/10.1179/cmq.2010.49.3.275.
[20] A. Ilbagi, H. Henein, A.B. Phillion, Phase quantification of impulse atomized Al68.5Ni31.5 alloy, J. Mater. Sci. (2011) 6235–6242, https://doi.org/10.1007/s10853-010-4972-8. Springer.
[21] A. Ilbagi, P. Delshad Khatibi, I.P. Swainson, G. Reinhart, H. Henein, Microstructural analysis of rapidly solidified aluminium - nickel alloys, in: Can. Metall. Q, Maney Publishing, 2011, pp. 295–302, https://doi.org/10.1179/1879139511Y.0000000006.

[22] J.B. Wiskel, H. Henein, E. Maire, Solidification study of aluminum alloys using impulse atomization: part I - heat transfer analysis of an atomized droplet, Can. Metall. Q. 41 (2002) 97–110, https://doi.org/10.1179/cmq.2002.41.1.97.
[23] A.A. Bogno, J. Valloton, D.D. Jimenez, M. Rappaz, H. Henein, Rapid solidification of Al-Cu droplets of near eutectic composition, IOP Conf. Ser. Mater. Sci. Eng 529 (2019), https://doi.org/10.1088/1757-899X/529/1/012021.
[24] A.A. Bogno, H. Henein, D.G. Ivey, J. Valloton, G. Reinhart, D. Sediako, M. Gallerneault, Effects of scandium on rapid solidified hypo-eutectic aluminium copper, Can. Metall. Q. 59 (2020) 101–115, https://doi.org/10.1080/00084433.2019.1696606.
[25] W. Hearn, A.A. Bogno, J. Spinelli, J. Valloton, H. Henein, Microstructure solidification maps for Al-10 Wt Pct Si alloys, Metall. Mater. Trans. A Phys. Metall. Mater. Sci. 50 (2019) 1333–1345, https://doi.org/10.1007/s11661-018-5093-2.
[26] D.H. Xiao, M. Song, F.Q. Zhang, Y.H. He, Characterization and preparation of Mg-Al-Zn alloys with minor Sc, J. Alloys Compd. (2009), https://doi.org/10.1016/j.jallcom.2009.04.113.
[27] J. Röyset, Scandium in Aluminium Alloys Overview: Physical Metallurgy, Properties and Applications, 2007.
[28] C.-H. Joh, K. Yamada, Y. Miura, Effect of Sc-Addition on the coarsening behavior of Al₃Li precipitates in Al–Li alloys, Mater. Trans. JIM 40 (1999) 439–442, https://doi.org/10.2320/matertrans1989.40.439.
[29] M. Trybula, T. Gancarz, W. Gasior, A. Pasturel, Bulk and surface properties of liquid Al-Li and Li-Zn alloys, Metall. Mater. Trans. A Phys. Metall. Mater. Sci (2014), https://doi.org/10.1007/s11661-014-2524-6.
[30] T. Gancarz, W. Gąsior, H. Henein, The discharge crucible method for making measurements of the physical properties of melts: an overview, Int. J. Thermophys. (2014), https://doi.org/10.1007/s10765-014-1748-4.
[31] H. Henein, Single fluid atomization through the application of impulses to a melt, Mater. Sci. Eng. A 326 (2002) 92–100, https://doi.org/10.1016/S0921-5093(01)01429-0.
[32] Standard Test Methods for Metal Powders and Powder Metallurgy Products, M.P.I. Federation, 2012.
[33] T. Gancarz, G. Cempura, Characterization of ZnAl cast alloys with Li addition, Mater. Des. (2016), https://doi.org/10.1016/j.matdes.2016.05.019.
[34] M.E. Trybula, T. Gancarz, W. Gasior, Density, surface tension and viscosity of liquid binary Al-Zn and ternary Al-Li-Zn alloys, Fluid Phase Equilib. (2016), https://doi.org/10.1016/j.fluid.2016.03.013.
[35] M.J. Assael, K. Kakosimos, R.M. Banish, J. Rgen Brillo, I. Egry, R. Brooks, P. N. Quested, K.C. Mills, A. Nagashima, Y. Sato, W.A. Wakeham, Reference Data for the Density and Viscosity of Liquid Aluminum and Liquid Iron, 2006, https://doi.org/10.1063/1.2149380.
[36] A.B. Spierings, K. Dawson, T. Heeling, P.J. Uggowitzer, R. Schäublin, F. Palm, K. Wegener, Microstructural features of Sc- and Zr-modified Al-Mg alloys processed by selective laser melting, Mater. Des. (2017), https://doi.org/10.1016/j.matdes.2016.11.040.
[37] T. Gancarz, J. Jourdan, W. Gasior, H. Henein, Physicochemical properties of Al, Al-Mg and Al-Mg-Zn alloys, J. Mol. Liq. 249 (2018), https://doi.org/10.1016/j.molliq.2017.11.061.
[38] W.F. Gale, T.C. Totemeier (Eds.), Smithells Metals Reference Book, 8th editio, Butterworth-Heinemann, 2003.
[39] N.A. Belov, D.G. Eskin, A.A. Aksenov, Multicomponent Phase Diagrams: Applications for Commercial Aluminum Alloys, 1st editio, Elsevier, 2005.
[40] E. Schürmann, I. Geissler, Solid phase equilibrium in Mg-rich alloys of the Al–Li–Mg system, Giessereiforschung 32 (1980) 163–174.
[41] E. Schürmann, H. Voss, Investigation of the melting equilibria of Mg-Li-Al alloys, Giessereiforschung 33 (1981) 33–53.
[42] M.E. Drits, E.M. Padezhnova, L.S. Guzei, The Mg–Li–Al phase diagram, Russ. Metall. 2 (1977) 167–170.
[43] L. Rokhlin, Ternary Alloy Systems - Phase Diagrams, Crystallographic and Thermodynamic Data: Light Metal Systems, Part 3: Selected Systems from Al-Fe-V to Al-Ni-Zr, Landolt-Börnstein, 2005, pp. 178–186, https://doi.org/10.1007/b96194.
[44] A.A. Nayeb-Hashemi, J.B. Clark, A.D. Pelton, The Li-Mg (Lithium-Magnesium) system, Bull. Alloy Phase Diagr. 5 (1984) 365–374, https://doi.org/10.1007/BF02872951.
[45] N.C. Goel, J.R. Cahoon, The Al-Li-Mg system (Aluminum-Lithium-Magnesium), Bull. Alloy Phase Diagr. 11 (1990) 528–546, https://doi.org/10.1007/BF02841712.
[46] R.H. Taylor, S. Curtarolo, G.L.W. Hart, Ordered magnesium-lithium alloys: first-principles predictions, Phys. Rev. B - Condens. Matter Mater. Phys (2010), https://doi.org/10.1103/PhysRevB.81.024112.
[47] Y. Peng, A. Chen, L. Zhang, W. Liu, G. Wu, Effect of Solution Treatment on Microstructure and Mechanical Properties of Cast Al-3Li-1.5Cu-0.2Zr Alloy, 2016, https://doi.org/10.1557/jmr.2016.103.
[48] B. Dubost, P. Bompard, I. Ansara, Experimental study and thermodynamic calculation of the Al-Li-Mg equilibrium phase diagram, Le J. Phys. Colloq 48 (1987) C3–473-C3-479, https://doi.org/10.1051/jphyscol:1987354.
[49] T. Himemiya, Micro-Segregation along the Monovariant Line in a Ternary Eutectic Alloy System. https://www.jim.or.jp/journal/e/pdf3/44/05/811.pdf, 2003 accessed July 5, 2021.
[50] S.W. Chen, Y.Y. Chuang, Y. Austin Chang, M.G. Chu, Calculation of phase diagrams and solidification paths of Al-rich Al-Li-Cu alloys, Metall. Trans. A. 22 (1991) 2837–2848, https://doi.org/10.1007/BF02650244.
[51] I. Konyashin, F. Lachmann, B. Ries, A.A. Mazilkin, B.B. Straumal, Strengthening Zones in the Co Matrix of WC – Co Cemented Carbides. Scripta Materialia 83, Elsevier, 2014, pp. 17–20, https://doi.org/10.1016/j.scriptamat.2014.03.026.
[52] S. Zhou, Z. Zhang, M. Li, D. Pan, H. Su, X. Du, P. Li, Y. Wu, Effect of Sc on microstructure and mechanical properties of as-cast Al-Mg alloys, Mater. Des. 90 (2016) 1077–1084, https://doi.org/10.1016/j.matdes.2015.10.132.
[53] S. Lee, A. Utsunomiya, H. Akamatsu, K. Neishi, M. Furukawa, Z. Horita, T. G. Langdon, Influence of scandium and zirconium on grain stability and superplastic ductilities in ultrafine-grained Al-Mg alloys, Acta Mater. (2002), https://doi.org/10.1016/S1359-6454(01)00368-8.
[54] I.N. Fridlyander, L.L. Rokhlin, T.V. Dobatkina, N.I. Nikitina, Investigation of the phase equilibria in aluminum alloys containing lithium, Met. Sci. Heat Treat. 35 (1993) 567–571, https://doi.org/10.1007/BF00778667.
[55] K. Dám, P. Lejček, A. Michalcová, In situ TEM investigation of microstructural behavior of superplastic Al-Mg-Sc alloy, Mater. Charact. 76 (2013) 69–75, https://doi.org/10.1016/j.matchar.2012.12.005.
[56] G.E. Thompson, B. Noble, Precipitation characteristics of aluminum-lithium alloys containing magnesium, J. Inst. Met. 101 (1973) 111–115.
[57] K.S. Prasad, N.E. Prasad, A.A. Gokhale, Microstructure and Precipitate Characteristics of Aluminum-Lithium Alloys, in: Aluminum-Lithium Alloy, Elsevier Inc., 2013, pp. 99–137, https://doi.org/10.1016/B978-0-12-401698-9.00004-5. Process. Prop. Appl.
[58] L.S. Kramer, T.J. Langan, J.R. Pickens, H. Last, Development of Al-Mg-Li alloys for marine applications, J. Mater. Sci. 29 (1994) 5826–5832, https://doi.org/10.1007/BF00366863.
[59] S. Kumar, H.B. McShane, T. Sheppard, Effect of zirconium and magnesium additions on properties of Al–Li based alloy, Mater. Sci. Technol. (United Kingdom). 10 (1994) 162–172, https://doi.org/10.1179/mst.1994.10.2.162.
[60] D.W. Levinson, D.J. McPherson, Phase relations in magnesium-lithium-aluminum alloys, Trans. Am. Soc. Met. 48 (1956) 689–705.
[61] J.C. Schuster, J. Bauer, The ternary systems ScAlN and YAlN, J. Less Common Met. 109 (1985) 345–350, https://doi.org/10.1016/0022-5088(85)90066-9.
[62] K. Kishio, J.O. Brittain, Phase stability of doped β-LiAl, Mater. Sci. Eng. 49 (1981) P1–P6, https://doi.org/10.1016/0025-5416(81)90144-0.
[63] T.V. Schegoleva, O.F. Rybalko, Структура Метастабильной S'-фасе в сплаве Al-Mg-Li, Fiz. Met. Metalloved. 50 (1980) 86–90.
[64] C. Suryanarayana, S.K. Tiwari, T.R. Anantharaman, A new metastable phase in the Aluminium-Magnesium System, Z. Metallkd. 69 (1978) 155–156.